Bakker A., Van den Akker H.E.A. (1990) Gas-Liquid Contacting with the Lightnin A315 Impeller, Effects of Flow Pattern. Presented at the AIChE Annual Meeting, November 11 to 16, 1990, Chicago, Session on Industrial Mixing and Scale-Up.

GAS LIQUID CONTACTING WITH THE LIGHTNIN A315 IMPELLER

Effects of flow-pattern

A. Bakker and H.E.A. van den Akker

ABSTRACT

This paper focuses on the gas-dispersion characteristics of modern hydrofoil impellers. Being a typical example of this class the Lightnin A315 was chosen for further study. The goal was to gain insight in the gas-dispersion properties of such hydrofoil impellers. Therefore the effects of impeller position and sparger geometry on flow pattern, power consumption and mass transfer have been studied in a vessel being 0.44 m in diameter, using liquids of different viscosity.

Different flow patterns and different types of cavities were found and were shown to be strongly related to the power consumption. Under certain conditions asymmetries and instabilities can occur. This can be explained in terms of the interaction between horizontal and vertical vortices. The sparger type influences both the power needed to prevent flooding and, at low power input, the mass transfer coefficient $k_l a$. The liquid viscosity does not affect the basic hydrodynamic phenomena in the vessel for viscosities not exceeding 80 mPas.

Prepared for presentation at:
AIChE annual meeting, November 11 to 16, 1990, Chicago
Session on Scale-up and Industrial Mixing II

Kramers Laboratorium voor Fysische Technologie
Delft University of Technology
Prins Bernhardlaan 6, 2628 BW Delft
The Netherlands

Date: November 1990

UNPUBLISHED

INTRODUCTION

Stirred reactors are often used for mixing of gases and liquids. Although traditionally many of these gas-liquid reactors are equipped with simple impellers like disc turbines or inclined blade impellers, which are cheap to make, so-called hydrofoil impellers have been developed during the last years. In general, the manufacturers of the latter claim that at a given power input these hydrofoil impellers are capable of dispersing more gas and of yielding higher mass-transfer coefficients than traditional impellers. As data in the open literature about these hydrofoil impellers are scarce, it is difficult to assess these claims.

This paper focuses on the gas-dispersion characteristics of such hydrofoil impellers. Being a typical example of this class the Lightnin A315 has been chosen for further study. The goal was to gain insight in the gas-dispersion properties of such hydrofoil impellers and to link the flow pattern and impeller hydrodynamics with power consumption and mass transfer. Therefore the effects of impeller position and sparger geometry on flow pattern, power consumption and mass transfer have been studied in a vessel being 0.44 m in diameter using liquids of different viscosity.

THEORY

Literature

Because of the industrial importance the hydrodynamics of gas-liquid stirred vessels have been the subject of extensive research (Nienow, 1990). Especially the hydrodynamical properties of the radially pumping Rushton turbine have been investigated thoroughly (Smith, 1985). The Rushton turbine is very effective in dispersing gas by breaking up the gas bubbles, but it has a relatively low hydraulic efficiency, which results in a low "flow per unit power". Further disadvantages of the Rushton turbine are the high levels of the shear stresses in the vicinity of the impeller, a non-uniform distribution of energy dissipation rate in the vessel (Laufhütte and

Mersmann, 1985) and a low gas-holdup in the lower part of the vessel (Mann and Hackett, 1986, Weetman, 1989).

Therefore research is shifting towards the properties of axially pumping impellers which have a higher hydraulic efficiency and effect a more uniform distribution of energy dissipation rate in the vessel. They further create lower shear stresses in the vicinity of the impeller. Axial flow impellers can be conveniently classified in two groups: simple impellers with flat inclined blades (pitched blade turbines), and so-called hydrofoil impellers with profiled blades. Examples of the latter are the Prochem hydrofoil and the Lightnin A315, both impellers looking very alike (fig. 1). It will be clear that axial flow impellers can be used pumping downwards as well as pumping upwards.

The use of pitched blade turbines for two-phase and three-phase mixing has been discussed by Chapman *et al.* (1983) who found that instabilities could occur when pitched blade turbines are used in the downwards pumping mode. Therefore these authors advised to use upwards pumping impellers, which were found to be more stable at high gassing rates.

Warmoeskerken *et al.* (1984) gave a description of the hydrodynamic properties and of the process of cavity formation with such pitched blade turbines. Two gas loading regimes were found: indirect loading and direct loading. Indirect loading occurs the gas is pumped downwards and enters the impeller only upon recirculation. At high gassing rates, however, the downward liquid flow will not be sufficiently strong to overcome and deflect the rising gas flow; hence the gas will rise directly into the impeller. This situation is called direct loading. These authors also reported that the mass transfer efficiency of a downwards pumping pitched blade turbine, based on the power demand, is at least as good as that of Rushton turbines.

Information about hydrofoil impellers in the open literature is relatively scarce. Oldshue (1988, 1989) reported that the A315 is capable of dispersing 86% more air than a disc turbine at the same power input and that mass transfer could be enhanced by 30% on the average by using an A315 system rather than a conventional disc turbine system. McFarlane (1989) studied the gassed flow pattern of the Prochem hydrofoil impeller; she found that instabilities occurred and that the gassed flow pattern could be

asymmetrical, but gave no explanation for this observation.

Bakker and Van den Akker (1990) compared a downwards pumping pitched blade turbine, a Lightnin A315 and a profiled Leeuwrik impeller (fig. 1) on basis of pumping efficiency, gas handling capacity and mass transfer. They found that the A315 had the highest pumping efficiency and was the most energy efficient with respect to dispersing the gas. Both the profiled Leeuwrik impeller and the A315 had a slightly better mass transfer performance than the downwards pumping pitched blade turbine.

Solidity ratio

According to Oldshue (1989) the solidity ratio of the impeller is an important parameter. The solidity ratio S_r is defined as the total blade area $n_b A_b$ (!) divided by the area of the circle that encloses the projection of the impeller onto a plane:

$$S_r = \frac{n_b A_b}{\frac{\pi}{4} D^2} \qquad (1)$$

An impeller with a high solidity ratio is capable of operating at a high pressure loading, which is advantageous in gas-liquid systems and in high viscosity fluids. Typical values for the solidity ratio are S_r = 90% for the A315 and S_r = 60% for a pitched blade turbine with six blades at 45° blade angle.

The advantage of a high solidity ratio can be described in more detail by looking at the thrust F_T delivered by the impeller. The thrust F_T induces a mean circulatory flow through the vessel, the strength of which strongly depends on the flow resistance. This resistance results from the vessel geometry (D/T ratio, bottom profile, impeller-bottom clearance, baffle design etc.). This resistance $\langle \Delta p_f \rangle$ therefore is taken proportional to the velocity head of a circulatory flow:

$$\langle \Delta p_f \rangle = K_w \frac{1}{2} \rho \langle v_{ax} \rangle^2 \qquad (2)$$

In addition, the thrust F_T is proportional to the thrust loading, $\langle \Delta p_b \rangle$, being the average pressure increase over the impeller from suction side to pressure side. Hence:

$$F_T = n_b A_{b,\perp} \langle \Delta p_b \rangle = \frac{\pi}{4} (D^2 - d_{hub}^2) \langle \Delta p_f \rangle \qquad (3)$$

and:

$$\langle \Delta p_b \rangle = \frac{F_T}{n_b A_{b,\perp}} = K_w \frac{1}{2} \rho \langle v_{ax} \rangle^2 \frac{\frac{\pi}{4} (D^2 - d_{hub}^2)}{n_b A_{b,\perp}} \qquad (4)$$

Here $A_{b,\perp}$ denotes the projected area of one blade. It is necessary to keep $\langle \Delta p_b \rangle$ as low as possible for two reasons. The first reason is that at a low $\langle \Delta p_b \rangle$ stalling will occur less easily. Stalling is the loss of pumping capacity due to separation of the boundary layer at the suction side of the impeller blade. The second reason is that due to the lower pressure at the suction side of the impeller blade, gas will accumulate there and this will eventually lead to the formation of large gas filled cavities and consequently to loss of pumping capacity. In case of a low $\langle \Delta p_b \rangle$ this will occur less easily and the impeller will be less sensitive to aeration. It will therefore be clear from eq. (4) that the projected blade area ratio $R_{b,\perp}$

$$R_{b,\perp} = \frac{n_b A_{b,\perp}}{\frac{\pi}{4} (D^2 - d_{hub}^2)} \qquad (5)$$

should be made as high as possible. This roughly corresponds with a high solidity ratio. The advantage of a large $R_{b,\perp}$ is confirmed by the fact that it has been repeatedly found that pitched blade turbines in gassed systems perform better when the number of blades is increased. For example Frijlink *et al.* (1990) found that six bladed inclined blade turbines performed better with respect to solids suspension in gassed systems than four bladed impellers.

EXPERIMENTAL SET-UP

A flat-bottomed perspex vessel of diameter T = 0.44 m was used in all experiments. The vessel was equipped with four baffles (width W = 0.1 T). The liquid height H was equal to the tank diameter T. Experiments were done with distilled water and glycerol solutions of viscosities η = 36 mPas and η = 80 mPas. The diameter of the A315 impeller was D = 0.4 T. The impeller was placed at a distance C = $\frac{3}{4}$ D from the vessel bottom, unless noted otherwise. The power demand was calculated from the impeller rotational speed and the torque exerted by the impeller. The torque was determined with a Vibro-torque transducer mounted in the shaft. Mass transfer experiments were done using a conventional dynamic method.

Several spargers were tested: a pipe sparger (PS), a small ring sparger (SRS, d_s = 0.4 D), a large ring sparger (LRS, d_s = 0.75 D) and a quadruple pipe sparger (QPS). The distance S between the ring spargers and the impeller could be varied. A schematic view of the spargers and the vessel can be found in figure 2. The quadruple pipe sparger (figure 3) is a Lightnin F30 sparge system look-alike.

HYDRODYNAMICS

The gassed flow pattern and impeller hydrodynamics

The gassed flow pattern as a function of impeller speed and the gassing rate has been studied visually. The process of cavity formation has been studied photographically. The results are illustrated in figure 4.

At low gassing rates and/or high impeller speeds, the gassed flow pattern is symmetrical, gas reaches the impeller only due to recirculation (indirect loading) and vortex cavities are formed (fig. 4A). If the impeller speed is decreased, or the gassing rate increased, the gas is still pumped downwards (indirect loading) but the impeller is not capable anymore of recirculating all the gas, the gas leaves the vessel on one side in a large gas cloud while on the other side it is recirculated in a small loop. In this case the flow pattern is asymmetrical and the gas cloud can be seen

precessing through the vessel with a period between approximately 1 and 30 minutes, depending on exact sparger geometry, gassing rate and power consumption. The direction of precession is the same as that of the impeller. In this situation growing cavities are formed (figure 4B). At still higher gassing rates the impeller is not capable of deflecting the rising gas flow and gas rises into the impeller directly (direct loading). In this situation large cavities are formed (figure 4C) and the flow pattern is dominated by the rising gas flow rather than by the impeller. This situation can also be called flooding. The transitions between the flow patterns are not sharp and often give rise to oscillations. Especially the indirect loading to direct loading transition was found to result in large torque fluctuations. This has already been observed for pitched blade turbines by Chapman *et al.* (1983).

The asymmetrical flow pattern

The precessing asymmetrical flow pattern depicted in figure 4B is quite interesting. Such asymmetries were already observed for other hydrofoil impellers (McFarlane, 1989) and can also be seen with pitched blade turbines. Further, these time dependent asymmetries have been observed on an industrial scale in the gold cyanidation process (Koen, 1990). This suggests that these asymmetries are inherent to all systems equipped with single axial flow impellers.

The mechanism behind this precessing asymmetrical flow pattern can be described in detail with the help of the sketch in figure 5. It is essential to understand that in a vessel equipped with an axial flow impeller two opposite kinds of vortex motion are interacting. The impeller induces both a tangential flow and an axial flow. Due to the tangential flow, vertical vortices are formed behind the baffles. On the other hand, the axial flow generates horizontal vortices lying near to the vessel bottom. The interaction between these horizontal and vertical vortices may lead to instabilities and an asymmetrical flow condition, depending on the ratio of the strength of the main, axial flow and the strength of the secondary, tangential flow.

At low gassing rates the impeller acts as an efficient pump and the flow

pattern in the vessel is dominated by the axial flow, and the associated circulation loops with the horizontal vortex in the center. Under these conditions instabilities may not get the opportunity to grow. At increasing gassing rate the pumping efficiency of the impeller decreases due to cavity formation: the strength of the axial flow induced by the impeller decreases faster than the strength of the tangential flow. At the same time, the momentum of the gas entering the vessel increases. The rising gas flow disturbs the recirculation loops and promotes and strengthens the long vertical vortices induced by the tangential flow. These effects together lead to the asymmetrical flow pattern depicted in figure 5. In this case the horizontal vortex caused by the axial flow lies near the bottom in front of baffle 1. Behind baffle 2 a vertical vortex is formed which bends sideways and joins with the horizontal vortex. Due to both the rising gas flow and the tangential flow caused by the impeller a strong vertical vortex is created behind baffle 3. The gas leaves the vessel in a cloud which roughly lies between baffle 3 and 4. There is no tangential vortex to be seen behind baffle 4 since the direction of rotation of this would-be vortex is opposed by the horizontal vortex in front of baffle 1. Due to the tangential motion induced by the impeller the diagonal vortex between baffle 2 and 3 is gradually bending more horizontal, towards baffle 3. At the same time the gas cloud from baffle 3 to 4 shifts gradually in the direction of baffle 4 to baffle 1 and the vertical vortex behind baffle 3 also bends gradually in the direction of baffle 4. Due to the fact that now a small vertical vortex behind baffle 4 is formed since more gas is rising up there the horizontal vortex in front of baffle 1 moves towards baffle 2, and joins with the vertical vortex behind baffle 3. As a consequence the whole flow pattern, including the rising gas cloud and the horizontal/vertical vortex system, slowly precesses in the direction of rotation of the impeller.

The period of precession depends on gassing rate, impeller speed, power consumption and sparger position. Typical values range from one minute to thirty minutes. Torque fluctuations, which have repeatedly been mentioned in literature, could be caused by oscillations in the strength of the different vortices and of course by oscillations between the different flow patterns near the indirect/direct loading transition. It should be noted that the

phenomena described above are not typical for the A315 impeller but were also observed with other axial flow impellers. Further, secondary flow loops and vortices can exist, depending on impeller type and probably also on scale, sparger configuration, D/T ratio and impeller-bottom clearance. But the present authors strongly believe that the horizontal/vertical vortex interaction described above is the main cause of asymmetries for all gassed vessels equipped with single axial flow impellers.

The link with power consumption

The gassed flow pattern, the power consumption and the impeller hydrodynamics are strongly related. Figure 6 shows the P_g/P_u curve at a constant impeller speed of $N = 5\ s^{-1}$. The different regions in this curve correspond with the three different flow patterns and types of cavities described before (see also figure 4). The formation of large cavities at the indirect/direct loading transition corresponds with a strong drop in power consumption.

The curves of the gassed power number Po_g vs. gas flow number Fl_g at a constant superficial gas velocity look quite different. Figure 7 shows the gassed power at three different superficial gas velocities for the large ring sparger. When at a certain gassing rate the impeller speed is increased, starting from a low speed (high Fl_g), Po_g decreases until a minimum is reached. This minimum corresponds with the indirect/direct loading transition. After the large cavities have disappeared at this critical flow number $Fl_{g,c}$, corresponding with a critical specific power consumption $\bar{\varepsilon}_c = P_c/V_l$, the power number increases at increasing impeller speed until a maximum is reached. When the impeller speed is increased even further Po_g decreases again, due to an increase in gas recirculation. When the quadruple pipe sparger is used these transitions are much smoother (fig. 8).

Sparger comparison

The performance of several spargers has been tested. Fig. 9 shows a comparison between the power curves for the small ring sparger (SRS) and the pipe sparger (PS). It is clear that the power drop in the curves occurs

earlier for the pipe sparger than for the ring sparger. This means that with the ring sparger less power is needed for dispersing a certain amount of gas.

Fig. 10 shows the effect of impeller to sparger separation distance S. When this distance is increased the power drop takes place at a higher gassing rate. Again this means that with respect to the power needed to disperse a certain amount of gas the larger separation distance is beneficial.

Figure 11 shows a comparison between the small ring sparger and the large ring sparger (LRS) for a liquid viscosity of η = 36 mPas. The steepest power drop occurs for the smaller ring sparger and the smaller separation distance. The minimum power consumption $\bar{\varepsilon}_c$ necessary for preventing the impeller from flooding has been determined as a function of gassing rate for the quadruple pipe sparger (QPS) and the large ring sparger mounted at S = 0.6 D (fig. 12). It is clear that at low gassing rates there is hardly any difference between these two sparger configurations but that at high superficial gas velocities the QPS performs better than the LRS.

In general it can be concluded that less power is needed to prevent the impeller from flooding when the gas input is moved outwards or further away from the impeller (fig. 2). This may be attributed to two effects. At first it may be clear that when the sparger is moved outwards and/or downwards this will lead to a lower gas holdup below the impeller. This results in a lower static pressure difference which has to be overcome by the impeller; as a consequence flooding will occur less easily. The second effect is related to the momentum of the input gas. The rising gas will induce an upward fluid motion, which opposes the downward flow below the impeller. This effect will be less when the gas is supplied closer to the vessel bottom.

Influence of liquid viscosity

The Po_g vs. Fl_g curves have been measured for different liquid viscosities, for the LRS mounted at an impeller to sparger separation distance S = 0.6 D (fig. 13). It turns out that the basic shape of the curves does not change significantly and that only the exact positions of the minima and the maxima change. Hence it can be concluded that the hydrodynamic processes in the

vessel are the same for liquid viscosities ranging from η = 1 mPas to η = 80 mPas.

It is quite interesting to see that for the large ring sparger mounted at S = 0.6 D, the critical power consumption $\bar{\varepsilon}_c = P_c/V_l$ increases almost linearly with liquid viscosity within the investigated range (fig. 14).

MASS TRANSFER

The mass transfer coefficient $k_l a$ has been determined using a conventional dynamic measurement method. The experiments were performed in distilled water. The superficial gas velocity was v_{sg} = 0.01 m/s. The quadruple pipe sparger (QPS) and the larger ring sparger (LRS) placed at S = 0.6 D were compared.

Bakker and Van den Akker (1990) investigated the influence of the impeller to bottom clearance on $k_l a$. They found that $k_l a$ increased when the clearance was decreased from C/D = 1.0 to C/D = 0.75. This was thought to be due to an increase in gas holdup in the lower part of the vessel. The mass transfer experiments reported in this paper were therefore performed with the impeller mounted at a clearance C/D = 0.75.

The results are plotted in figure 15. It is clear that at low power consumptions the LRS yields a slightly larger $k_l a$ value than the QPS. This is possibly due to the lower gas holdup below the impeller when using the QPS. It should be noticed that the difference in overall gas holdup between the two spargers may be small, but since the local energy dissipation rate below the impeller will be relatively large, k_l will also be large in this region. A small increase in hold-up below the impeller, caused by using a smaller sparger mounted close to the impeller, may therefore result in a significant increase in $k_l a$.

As the power consumption is increased, and the gas recirculation rate increases, the difference between the QPS and the LRS gets smaller, until at specific power consumptions $\bar{\varepsilon} = P/V_l$ in excess of 2500 W/m^3 the gas holdup below the impeller is fully determined by the recirculation rate instead of by the sparger position; thus no significant difference in $k_l a$ is found between the two spargers.

CONCLUSIONS

The hydrodynamic properties of the A315 impeller have been investigated. Different flow patterns and different types of cavities were found and were shown to be strongly related to the power consumption. These flow patterns and the hydrodynamic regime of the impeller basically did not change in the investigated range of liquid viscosities between η = 1 mPas and η = 80 mPas. The minimum power consumption to prevent the impeller from flooding, however, showed an almost linear increase with liquid viscosity.

Asymmetrical flow patterns were found, which can also be seen with other axial flow impellers, and the mechanism behind this phenomenon has been described in terms of the interaction between horizontal and vertical vortices.

The advantage of a large solidity ratio S_r has been explained in detail by looking at the average pressure difference over the impeller blades.

Different sparger types have been compared. It turns out that less power is needed to disperse the gas when the gas inlet is moved outwards and/or closer to the vessel bottom. Those sparger configurations which are most effective in dispersing the gas, however, were found to yield a slightly lower mass transfer coefficient k_la than other sparger configurations. At high specific power consumptions this difference in k_la vanishes again. A 0.75 D ring sparger mounted at a separation distance S = 0.6 D is a good compromise between gas handling capacities and mass transfer performance.

Above conclusions are by no means restricted to the A315 impeller, but basically hold for all gassed stirred vessels equipped with one single axial flow impeller.

ACKNOWLEDGEMENTS

These investigations are supported by the Netherlands Technology Foundation (STW, DTN 40.0566).

The authors would like to thank student M. Goedemans for his help in performing the experiments.

The A315 impeller was kindly put at our disposal by Mixing Equipment Co.

NOMENCLATURE

Symbols

$A_{b,\perp}$	= Projected area of one impeller blade	(m^2)
A_b	= Area of one impeller blade	(m^2)
C	= Impeller to bottom clearance	(m)
d_{hub}	= Impeller hub diameter	(m)
d_S	= Sparger diameter	(m)
D	= Impeller diameter	(m)
F_T	= Axial force exerted by the impeller (thrust)	(N)
Fl_g	= Gas flow number (= Q_g/ND^3)	(-)
H	= Liquid height	(m)
k_l	= Partial mass transfer coefficient	(m/s)
k_la	= Overall volumetric mass transfer coefficient	(s^{-1})
K_W	= Friction coefficient	(-)
N	= Impeller speed	(s^{-1})
n_b	= Number of impeller blades	(-)
P	= Power consumption	(W)
Po	= Impeller power number (= $P/\rho N^3D^5$)	(-)
Q_g	= Gassing rate	(m^3s^{-1})
$R_{b,\perp}$	= Projected blade area ratio	(-)
S	= Impeller-sparger separation	(m)
S_r	= Solidity ratio	(-)
T	= Vessel diameter	(m)
v_{sg}	= Superficial gas velocity	(ms^{-1})
$\langle v_{ax} \rangle$	= Average axial liquid velocity out of the impeller plane	(ms^{-1})
V_l	= Liquid volume	(m^3)
W	= Baffle width	(m)
$\langle \Delta p_f \rangle$	= Average pressure rise at impeller	(Pa)
$\langle \Delta p_b \rangle$	= The average pressure difference between the two sides of an impeller blade	(Pa)
$\bar{\varepsilon}$	= Average energy dissipation rate (= P/V_l)	(W/m^3)
ρ	= Liquid density	(kgm^{-3})
η	= Liquid viscosity	(mPas)

Subscripts

g = gassed

u = ungassed

c = critical, at the indirect/direct loading transition

LITERATURE

Bakker A., Van den Akker H.E.A., 1990, Proceedings Fluid Mixing IV, Organized by IChemE in Bradford U.K., september 11-13 1990, 153-166.

Chapman C.M., Nienow A.W., Cooke M., Middleton J.C., 1983, Chem.Eng.Res.Des. 61, 71-95 and 167-185.

Frijlink J.J., Bakker A., Smith J.M., 1990, Chem.Eng.Sci. 45, No 7, 1703-1718

Koen C., 1990, personal communication

Laufhütte H.D., Mersmann A.B., 1985, Proceedings 5th. Eur.Conf.Mixing, BHRA Fluid Engineering, Cranfield U.K., 331-340

Mann R., Hackett L.A., 1988, Proceedings 6th. Eur.Conf.Mixing, BHRA Fluid Engineering, Cranfield U.K., 321-328

McFarlane C., 1989, MIXING XII, Organised by the Engineering Foundation, Trout Lodge U.S.A., Unpublished

Nienow A.W., 1990, Chemical Engineering Progress, February 1990, 61-71

Oldshue J.Y., Post T.A., Weetman R.J., Coyle C.K., 1988, Proceedings 6th. Eur.Conf.Mixing, BHRA Fluid Engineering, Cranfield U.K., 345-350

Oldshue J.Y., 1989, Chemical Engineering Progress 5, 33-42

Smith J.M., 1985, "Dispersion of gases in liquids", in "Mixing of liquids by mechanical agitation", Eds. Ulbrecht J.J and Patterson G.K., Gordon and Breach Science Publishers, ISSN: 0734-1644, ISBN: 2-88124-112-3

Weetman R.J., 1989, European Patent Application 89109743.8

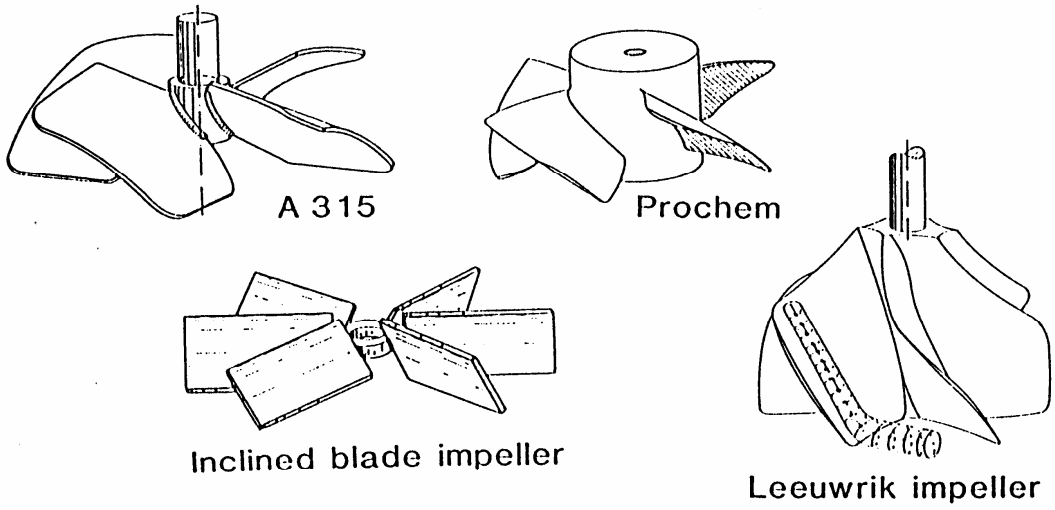

Figure 1 Four different axial flow impellers.

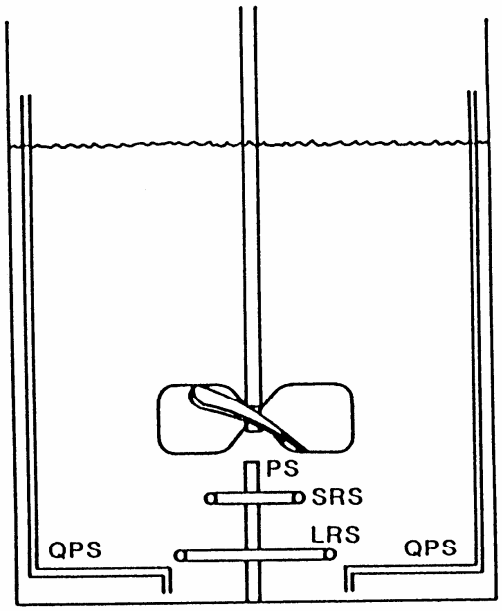

Figure 2 The four investigated sparger types, a pipe sparger (PS), a small ring sparger (SRS), a large ring sparger (LRS) and a quadruple pipe sparger (QPS).

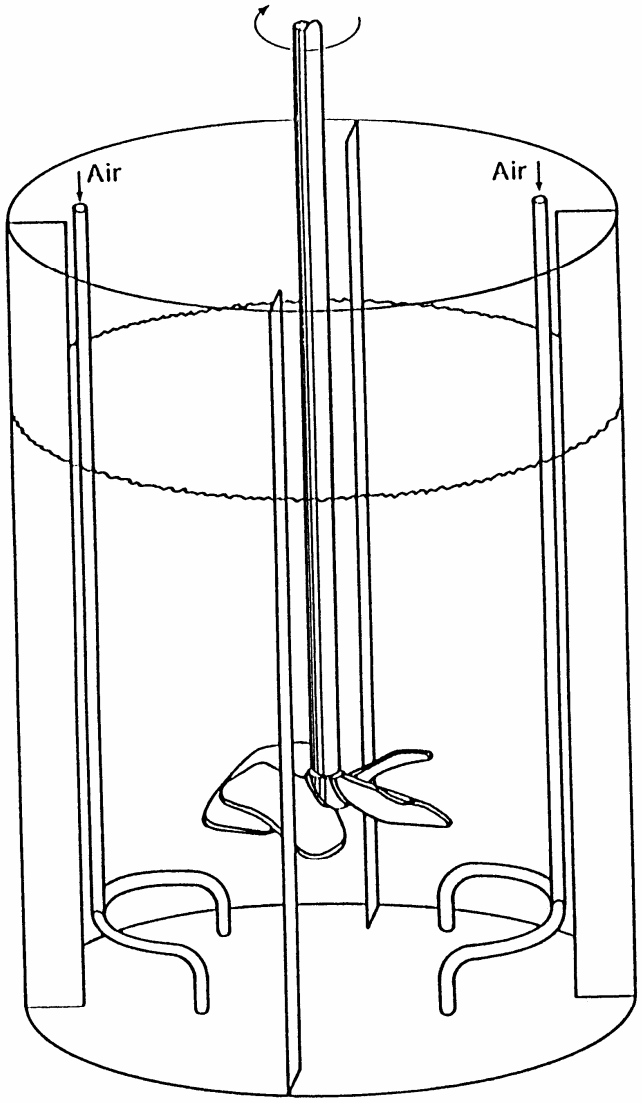

Figure 3 A 3-dimensional view of the quadruple pipe sparger. This type of sparger is also available from Lightnin as a F30 sparge system.

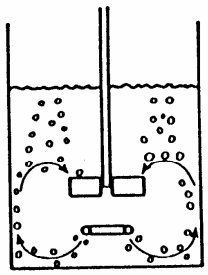

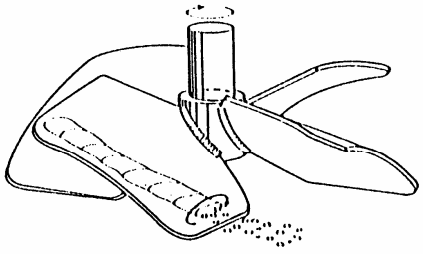

A. Indirect loading, symmetrical flow pattern

vortex cavity

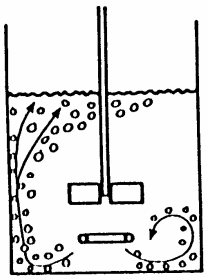

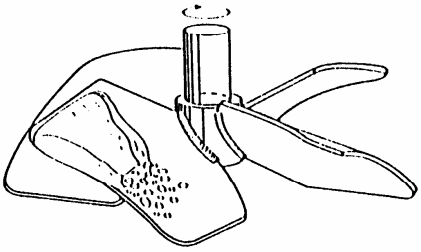

B. Indirect loading, precessing asymmetrical flow pattern

growing cavity

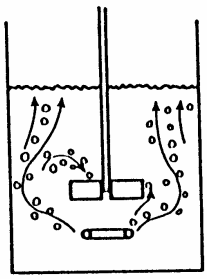

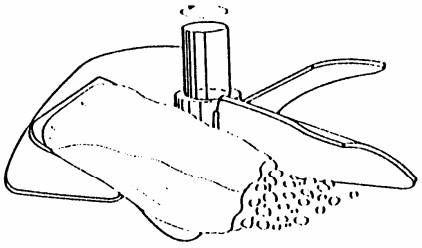

C. Direct loading

large cavity

Figure 4a,b,c The relationship between the three possible flow patterns and the cavity formation process.

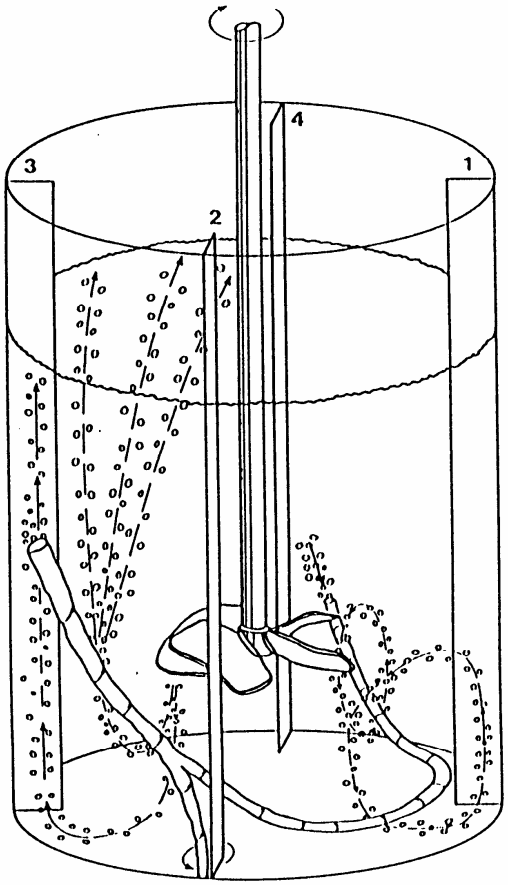

Figure 5a The vortex system which causes the asymmetrical flow pattern, 3-dimensional view.

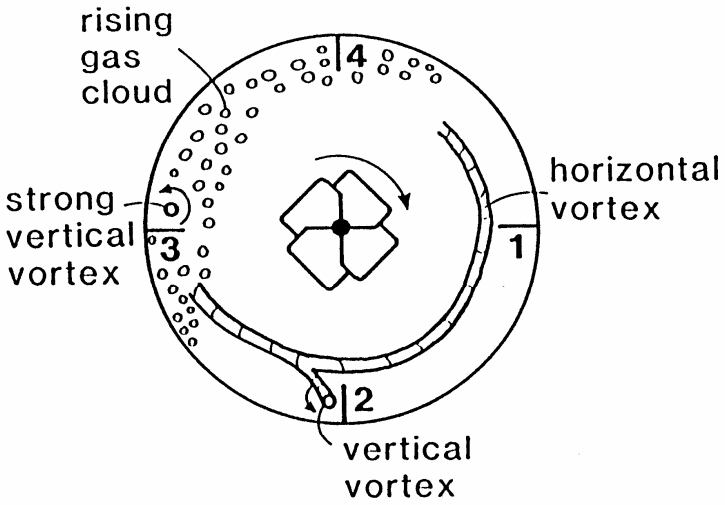

Figure 5b The vortex system which causes the asymmetrical flow pattern, top view.

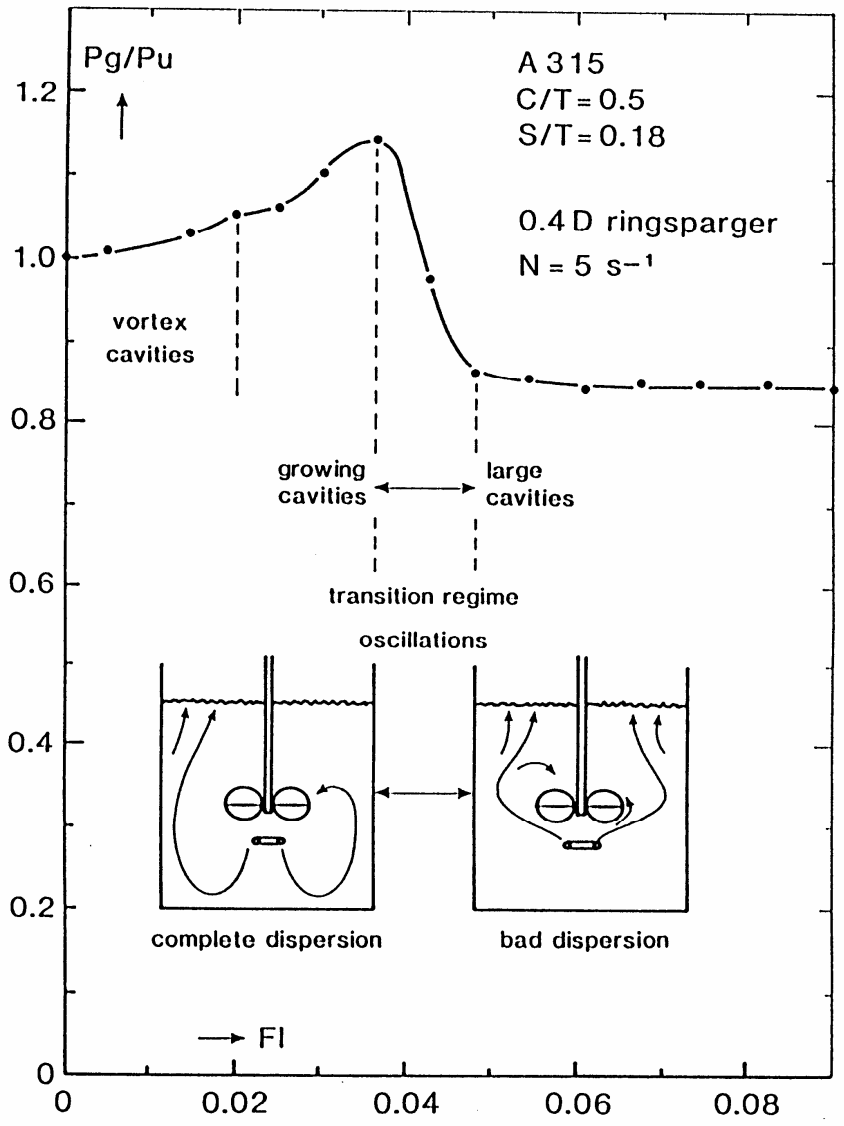

Figure 6 The gassed power consumption, the gassed flow patterns and the cavity formation process related.

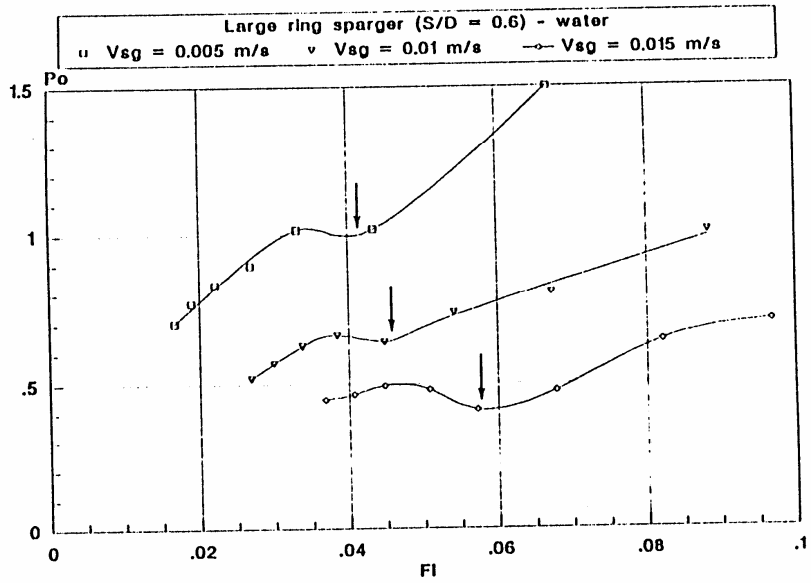

Figure 7 The gassed power curves for the large ring sparger. The indirect to direct loading transition is marked by arrows.

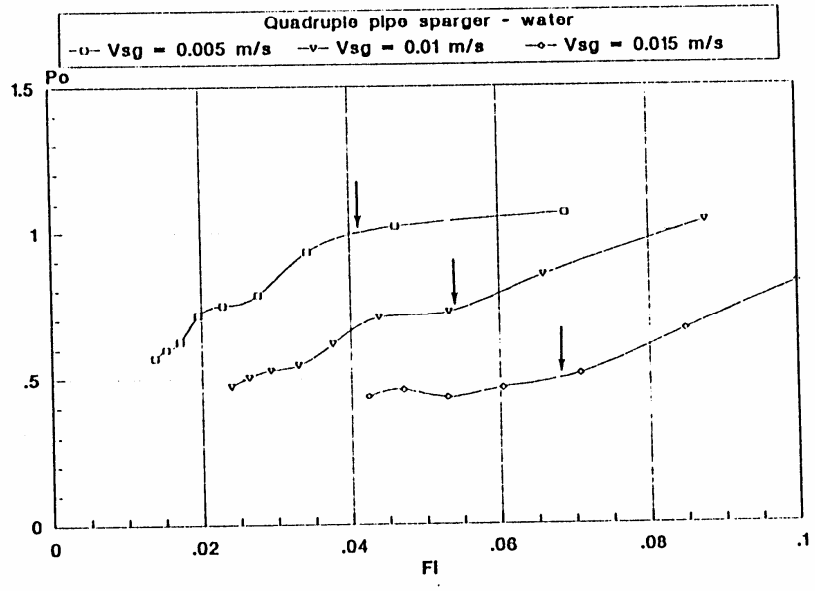

Figure 8 The gassed power curves for the quadruple pipe sparger. The indirect to direct loading transition is marked by arrows.

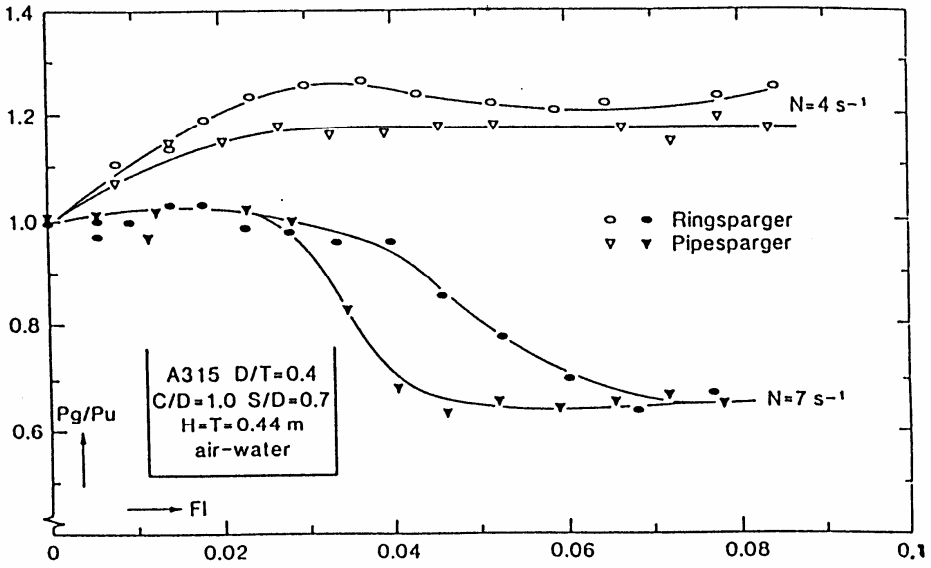

Figure 9 The gassed power curves for the small ring sparger and the pipe sparger.

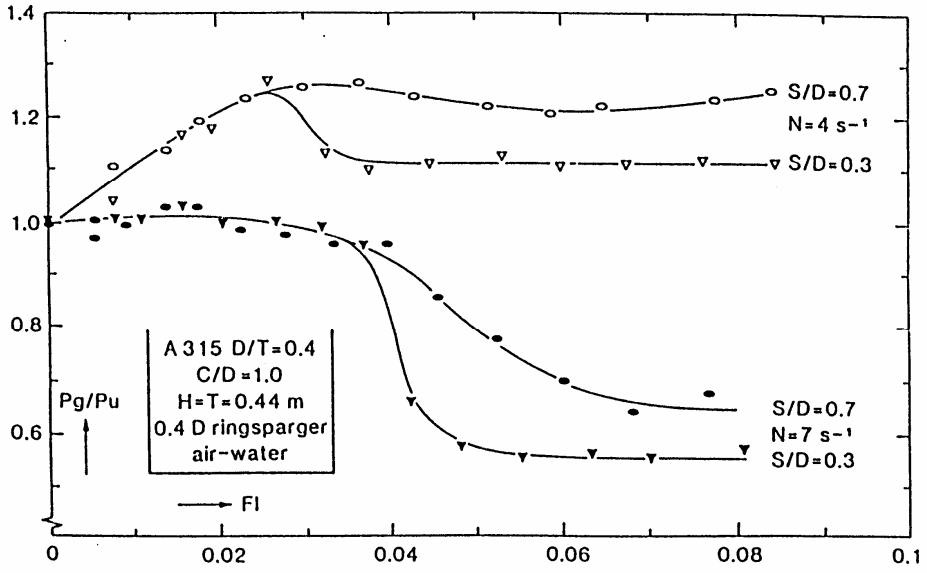

Figure 10 The gassed power curves for the small ring sparger at two different impeller-sparger separation distances.

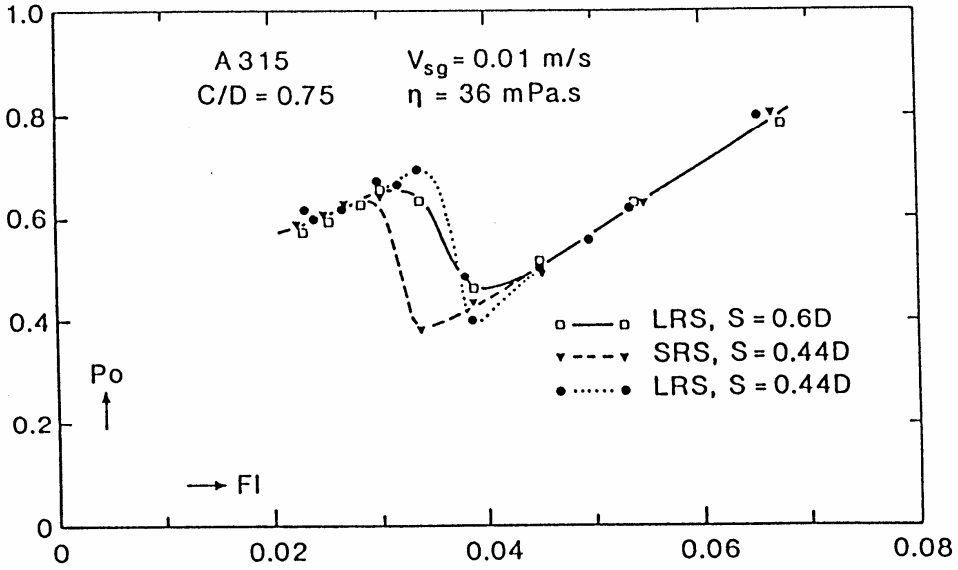

Figure 11 The gassed power curves at a liquid viscosity of η = 36 mPas for three different sparger configurations.

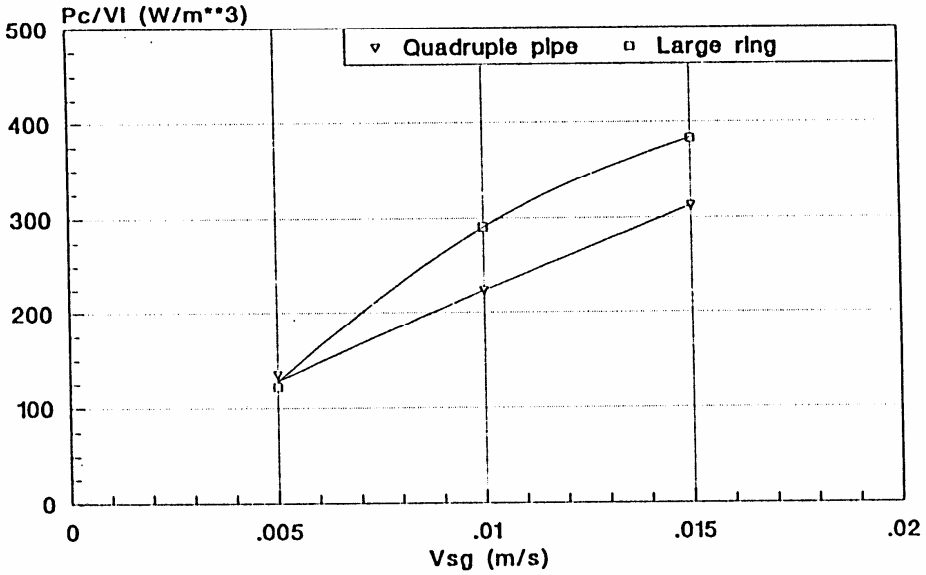

Figure 12 The minimum power consumption to prevent direct loading for the quadruple pipe sparger and the large ring sparger.

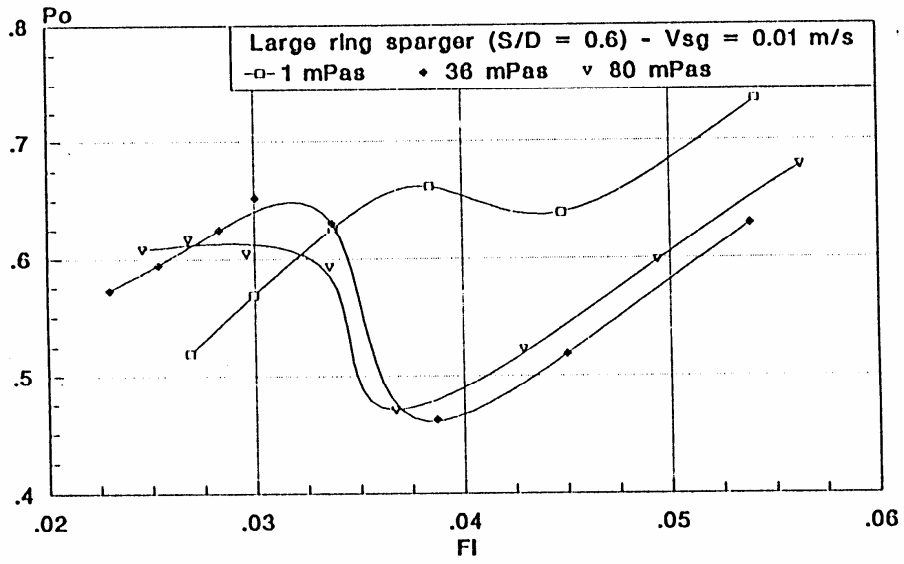

Figure 13 The power curves for the large ring sparger at three different liquid viscosities.

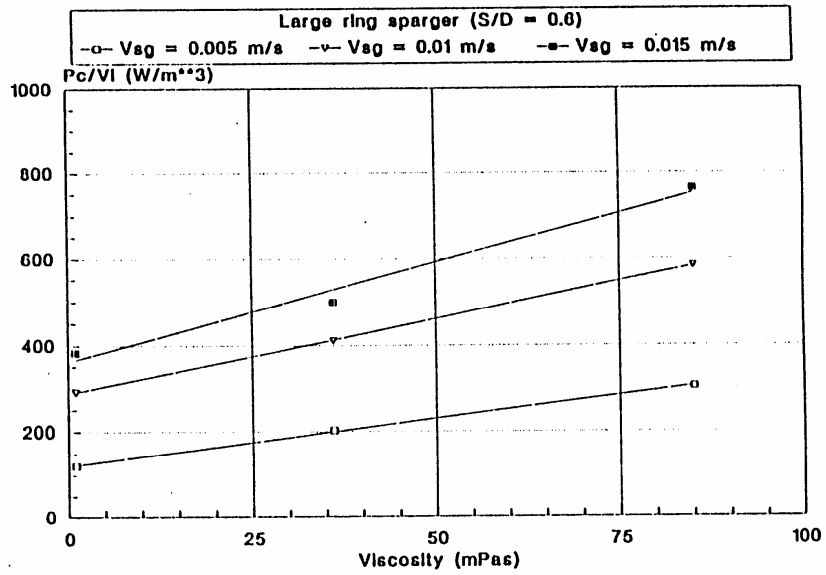

Figure 14 The minimum power consumption to prevent direct loading as a function of liquid viscosity for the large ring sparger.

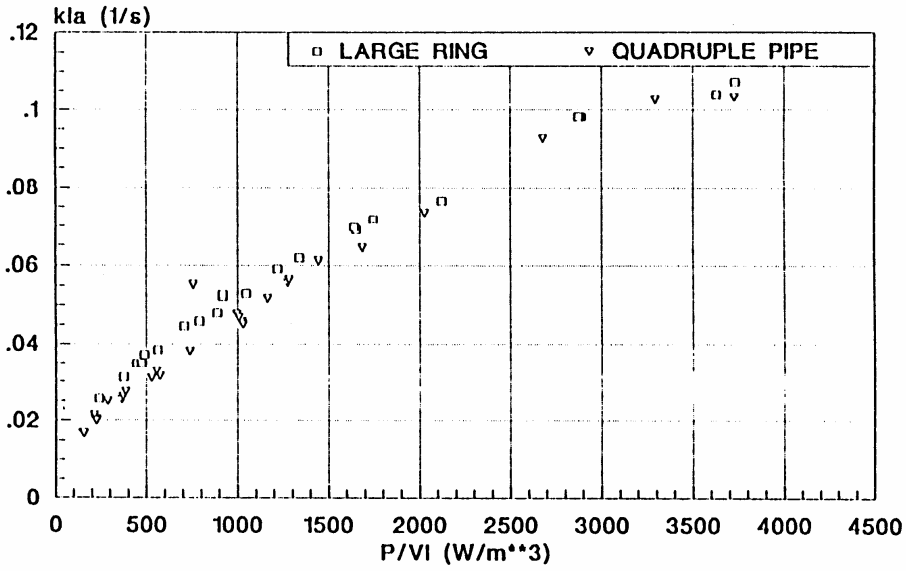

Figure 15 The mass transfer coefficient $k_l a$ as a function of power input for the quadruple pipe sparger and the large ring sparger.

****APPENDIX****

GAS LIQUID CONTACTING WITH THE LIGHTNIN A315 IMPELLER

Effects of flow-pattern

A. Bakker and H.E.A. van den Akker

Mass Transfer

Figure 15 in the paper shows the mass transfer coefficient $k_l a$ as a function of the power consumption for the large ringsparger and the quadruple pipesparger. Figure 16 (appendix) also includes data for the small ringsparger (S/D = 0.5). This graph confirms the statement in the paper that at low power consumptions $k_l a$ increases at decreasing sparger diameter and decreasing sparger-impeller separation distance.

Solids suspension

Figure 17 (appendix) shows the minimum power consumption for solids suspension according to the Zwietering 1 second criterion as a function of superficial gas velocity. Three impeller types are compared: an upward pumping inclined blade impeller (45U6), a downward pumping inclined blade impeller (45D6) both at C/T = 0.25, with a small ringsparger (d_s/D = 0.4) at S/T =0.25 and with six blades (width B_w/D = 0.2) and an A315 (C/T = 0.3, d_s/D =0.75, S/D = 0.6). The A315 has the best overall performance.

Local gas holdup

The local gas holdup has been measured with an optical fiber probe for two different sparger types at the same power consumption and superficial gas velocity (see color plot in figure 18; red: high holdup; blue: low holdup; black dots: spargers). It is clear that the gas holdup below the impeller is strongly influenced by the sparger position and sparger size. The overall gas holdup is slightly higher for the small sparger mounted close to the impeller. This confirms the higher $k_l a$ values found for this small sparger. It is also interesting to see that the gas enters the impeller relatively from the side, and that the gas is dispersed from the trailing vortex.

FIGURE 16 (MASS TRANSFER)

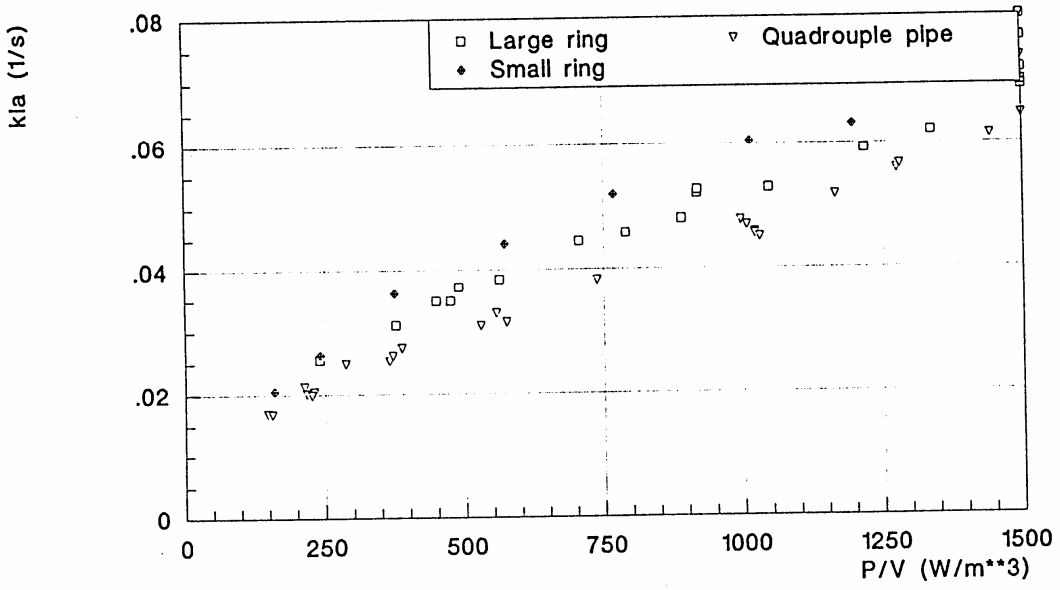

A315 - sparger comparison at Vsg = 0.01 m/s

FIGURE 17 (SOLIDS SUSPENSION)

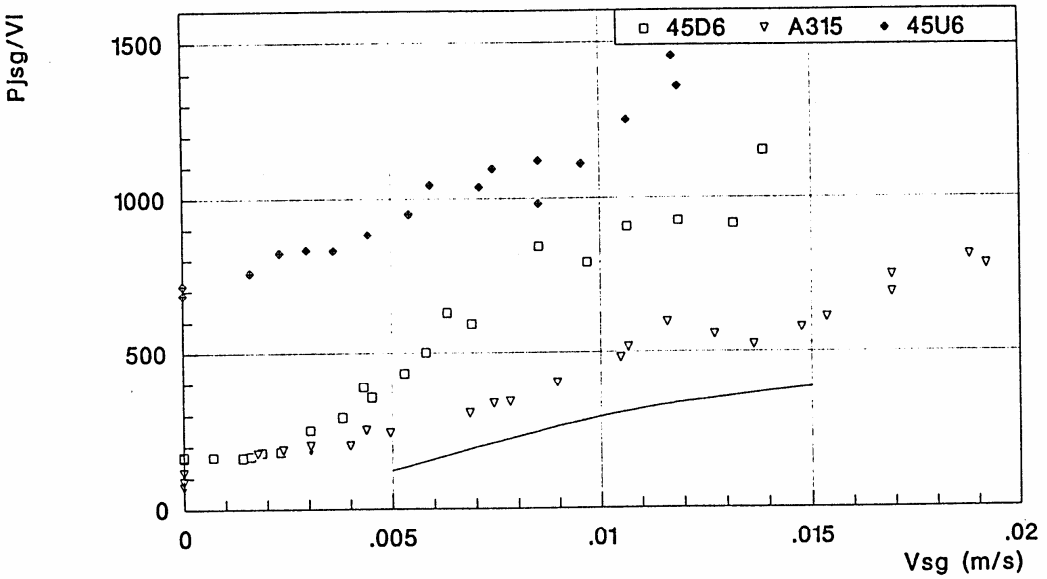

The line indicates the indirect/direct loading transition for the A315
The experiments were performed with 1 mass% solids.

FIGURE 18 (LOCAL GAS HOLDUP)